Some aspects of polarized line formation in magneto-turbulent media

M. Sampoorna [a,1] H. Frisch [b] K. N. Nagendra [a,*]

[a] *Indian Institute of Astrophysics, Koramangala, Bangalore 560 034, India*

[b] *Laboratoire Cassiopée (CNRS, UMR 6202), Observatoire de la Côte d'Azur, BP 4229, 06304 Nice Cedex 4, France*

Abstract

Observations and numerical simulations of magneto-convection show a highly variable solar magnetic field. Using a statistical approach, we analyze the effects of random magnetic fields on Stokes profiles of spectral lines. We consider the micro and macro-turbulent regimes, which provide bounds for more general random fields with finite scales of variations. The mean Stokes parameters are obtained in the micro turbulent regime, by first averaging the Zeeman propagation matrix $\hat{\mathbf{\Phi}}$ over the probability distribution function $P(\boldsymbol{B})$ of the magnetic field and then solving the concerned radiative transfer equation. In the macro-turbulent regime, the mean solution is obtained by averaging the emergent solution over $P(\boldsymbol{B})$. It is assumed that $\boldsymbol{B}$ has a Gaussian distribution defined by its mean field $\boldsymbol{B}_0$, angular distribution and dispersion. Fluctuations parallel and perpendicular to $\boldsymbol{B}_0$ are considered. Spectral lines are parameterized by their strength β, which is varied over the range 1 to 10^4. A detailed comparison of micro and macro-turbulent limit with mean field solution shows that differences are important for $\beta \geq 10$. When β increases, the saturation behavior of micro-turbulent profiles are significantly different from that of mean field profiles. The Stokes profiles shapes are explained in terms of the non-linear β-dependence of the Unno-Rachkovsky solution using approximate expressions for the mean absorption coefficients. These expressions when inserted in the Unno-Rachkovsky solution can predict Stokes profiles that match with the numerical result to a good approximation.

Key words: Stellar atmospheres: line formation, Stellar atmospheres: radiative transfer, Magnetic fields, polarization
PACS: 97.10.Ex, 97.10.Ex, 97.10.Ld

1. Introduction

Quantitative analysis of spectro-polarimetric data entered an active phase with the analytical solution of Unno (1956). This solution considers only the absorption/emission of polarized radiation in a magnetized medium. The extension by Rachkovsky (1962a, 1962b) includes magneto-optical effects due to differential shifts between orthogonal polarization states, which appear during the propagation through the medium. Magneto-optical effects are important when Zeeman shifts are of the order of Doppler widths and affect Stokes parameters mainly around the line center. The analytical solution of the Stokes vector transfer equation known as Unno–Rachkovsky solution (hereafter referred to as UR solution) implies a uniform magnetic field and approximations regarding the atmospheric model known as Milne–Eddington approximations - namely that the line strength is independent of the depth in the atmosphere, and that the line source function varies linearly with optical depth. The Milne-Eddington approximation has provided insight into the physical processes taking place in line formation. Its specific analytical character is its most powerful feature. A new area in the analysis of polarization spectra was opened with numerical solutions of the polarized radiative transfer equation for realistic atmospheres involving depth-dependent physical quantities. It started with the work by Beckers (1969), Wittman (1974), Landi Degl'Innocenti (1976). See Rees (1987) for a historical review.

However the UR solutions continue to be used in astrophysics, in particular in inversion codes aimed at the automatic reconstruction of magnetic fields and atmospheric parameters from large sets of polarimetric data (e.g. UNNO-FIT technique – Landi Degl'Innocenti & Landolfi 2004, p. 634 and references cited therein; Bellot Rubio 2006 and references cited therein). It can, as recently shown, provide a systematic approach to evaluate the sensitivity of Stokes profiles to atmospheric and magnetic

* Indian Institute of Astrophysics, Koramangala, Bangalore 560 034, India

Email address: knn@iiap.res.in (K. N. Nagendra).

[1] Joint Astronomy Program, Dept. of Physics, Indian Institute of Science, Bangalore 560 012, India

field parameters (Orozco Suárez & del Toro Iniesta 2007). Let us also mention that a widely used atlas of theoretical Stokes profiles was constructed with the help of UR solution (Arena & Landi Degl'Innocenti 1982). An excellent description of UR solution, extensions and practical applications, are presented in del Toro Iniesta (2003) and Landi Degl'Innocenti & Landolfi (2004).

In this work we present a systematic study of the UR solution for random magnetic fields. The UR solution, can be employed for random fields in two limiting regimes : (i) the regime of micro-turbulence in which the characteristic scale of variation of the random magnetic field is much smaller than a typical photon mean free-path, and (ii) the regime of macro-turbulence where one has the opposite situation. The micro-turbulent approach, suggested in Stenflo (1971), has been employed in e.g. Stenflo & Lindegren (1977), Sánchez et al. (1996). Multi-components models are special versions of the macro-turbulent limit (see e.g. Stenflo 1994 and references cited therein). Here we assume that the magnetic field fluctuations are described by a probability distribution function $P(\boldsymbol{B})$. In the micro-turbulent regime, the coefficients of the polarized transfer equation, in particular the Zeeman propagation matrix (also called absorption matrix), can be locally averaged over $P(\boldsymbol{B})$. Dolginov & Pavlov (1972) and Domke & Pavlov (1979) were the first to examine Zeeman line transfer for micro-turbulent magnetic fields and proposed explicit expressions for the mean values of the coefficients of the Zeeman propagation matrix. An up-to-date presentation of their results and some extensions can be found in Frisch et al. (2005; hereafter referred to as Paper I). In the macro-turbulent regime, the magnetic field is uniform over the region where the spectral line is formed but takes random values distributed according to $P(\boldsymbol{B})$. The averaging over $P(\boldsymbol{B})$ is performed on the emergent UR solution itself.

The micro and macro-turbulent limits cannot describe situations where the mean free path of photons is of the same order as the characteristic scale of variation of the magnetic field. This more general situation requires the solution of polarized radiative transfer equations with stochastic coefficients (Frisch et al. 2006a, hereafter referred to as Paper II; see also Frisch et al. 2007; Carroll & Kopf 2007). The corresponding mean Stokes parameters always lie between the micro and macro-turbulent limits. The latter have thus a significant interest for assessing the effects of random magnetic fields.

In this paper we examine the micro and macro-turbulent limits for isotropic and anisotropic Gaussian magnetic field distributions. The velocity field is assumed to be micro-turbulent, and uncorrelated to the magnetic field. The results are compared to the UR solution corresponding to the mean magnetic field, henceforth referred to as the mean field solution. The comparison is carried out for lines with different line strength $\beta = \kappa_{\rm l}/\kappa_{\rm c}$ ($\kappa_{\rm l}$ the frequency averaged line absorption coefficient, $\kappa_{\rm c}$ the continuum absorption coefficient). In a Milne–Eddington atmosphere β is a constant. The UR solution varies linearly with β when β is small or around unity, but non-linearly when β becomes large. We investigate in detail this non-linear behavior for turbulent magnetic fields.

In Sect. 2 we consider the micro-turbulent limit and in Section 3 the macro-turbulent limit for longitudinal and transverse propagation. In these sections and all the following ones, the results are shown for a residual Stokes vector $\boldsymbol{r} = (r_{\rm I}, r_{\rm Q}, r_{\rm U}, r_{\rm V})^{\rm T}$, independent of the slope of the source function. In Sect. 4 we compare micro and macro-turbulence effects for an arbitrary orientation of the mean field and in Sect. 5 we discuss mean Stokes profiles calculated with isotropic and anisotropic distributions. In Sect. 6 concluding remarks are given. An Appendix is devoted to describe the basic equations.

2. Micro-turbulence with isotropic Gaussian fluctuations

In the micro-turbulent limit, the Stokes parameters and residual Stokes vector defined in Eq. (A.5) can be calculated with the UR solution given in Eqs. (A.7) – (A.13) where all the absorption and dispersion coefficients are replaced by their averages over the probability distribution function (PDF) $P(\boldsymbol{B})$ of the vector magnetic field. In this paper we consider PDFs that are cylindrically symmetrical about the direction of a mean field $\boldsymbol{B}_0$. They are defined in a reference frame with the Z-axis along the mean field direction and then transformed to the line of sight reference frame with the Z-axis along the line of sight (see Fig. A.1). The transformation from the magnetic to the line of sight reference frame can be found in Frisch et al. 2007.

In this section we consider a random magnetic field with a mean value $\boldsymbol{B}_0$ and fluctuations that are Gaussian and isotropic (other angular distributions are considered in Sect. 5). The PDF may thus be written as

$$P(\boldsymbol{B})\, d\boldsymbol{B} = \frac{1}{\pi^{3/2}}\, e^{-(y_0^2+y^2)}\, e^{2y_0 y\cos\Theta}\, y^2\, dy\, \sin\Theta\, d\Theta\, d\Psi, \qquad (1)$$

where Θ is the angle between the vector magnetic field $\boldsymbol{B}(\theta,\phi)$ and the mean magnetic field $\boldsymbol{B}_0(\theta_0,\phi_0)$ and Ψ the azimuth of $\boldsymbol{B}$ in a magnetic reference frame in which the Z-axis is taken along $\boldsymbol{B}_0$. The non-dimensional quantities y and y_0 are defined as $y = B/(\sqrt{2}\sigma)$, and $y_0 = B_0/(\sqrt{2}\sigma)$, with σ being the rms fluctuation given by $3\sigma^2 = \langle(\boldsymbol{B} - \boldsymbol{B}_0)^2\rangle$. Two important parameters of the model are $\Delta_Z B_0$ and $\gamma_B = \Delta_Z\sqrt{2}\sigma$, the Zeeman shifts due to the mean magnetic field and to the rms fluctuations (measured in Doppler width units). Here $\Delta_Z = ge/(4\pi mc\Delta\nu_{\rm D})$, with g the Landé factor and $\Delta\nu_{\rm D}$ the Doppler width which includes thermal and micro-turbulent velocity broadening (see e.g. Mihalas 1978; also Paper I). The ratio $f = 1/y_0 = \gamma_B/\Delta_Z B_0$ is a measure of the strength of the fluctuations, with large and small values of f corresponding to strong and weak turbulence respectively.

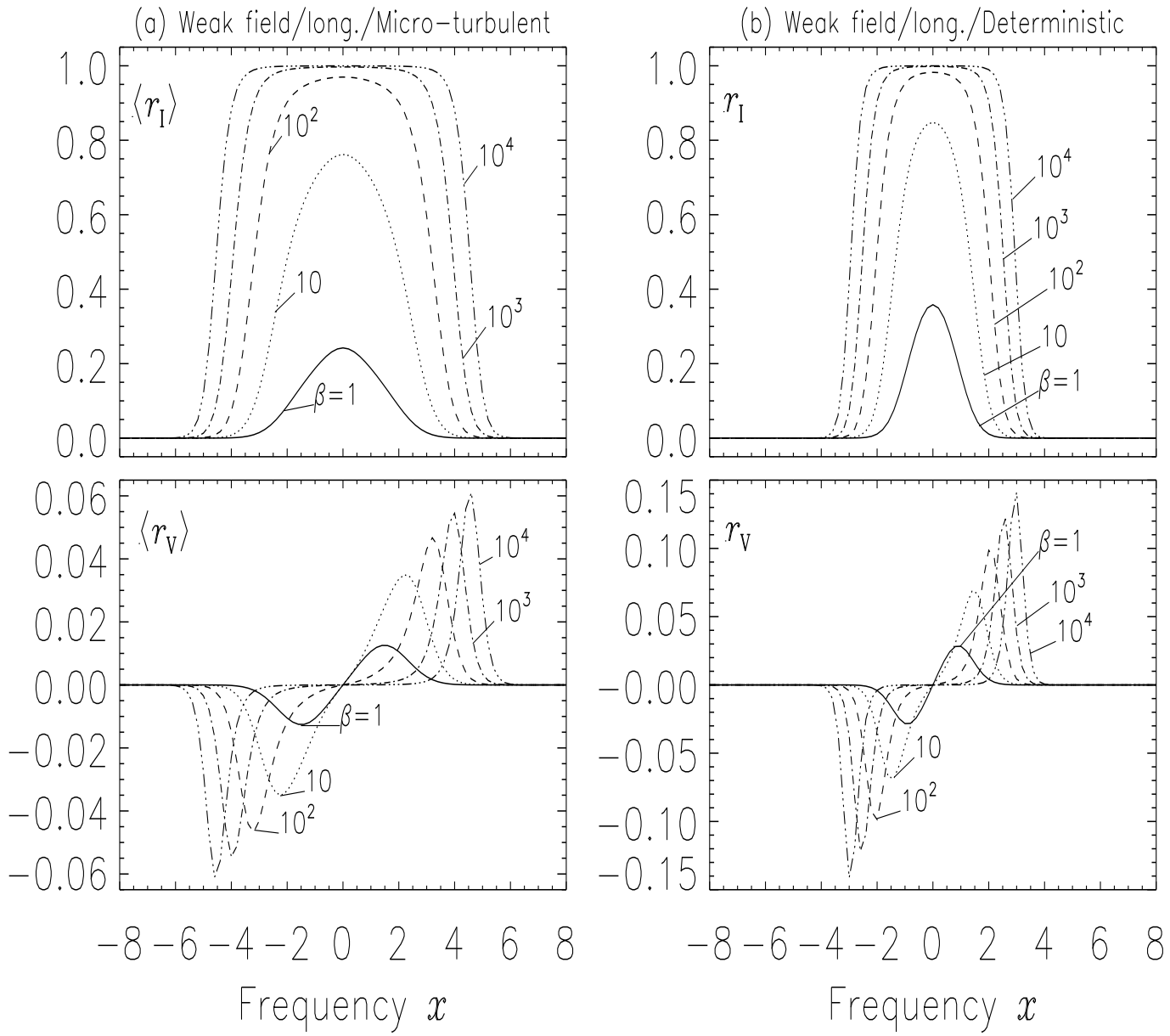

Fig. 1. Weak mean field limit. Dependence of $\langle r_{\rm I}\rangle$, and $\langle r_{\rm V}\rangle$ on line strength β for $a = 0$, $\theta_0 = 0°$. Panel (a) : micro-turbulent limit with $\Delta_Z B_0 = 0.1$, $\gamma_B = 1$ hence $y_0 = 0.1$ and $f = 10$. Panel (b) : deterministic case with $\Delta_Z B = 0.1$. Frequency x in Doppler width units. See Sect. 2.1 for discussions.

For a micro-turbulent magnetic field, the Doppler broadening is replaced by a combination of thermal, velocity and magnetic broadening described by the parameter $\gamma_1 = \sqrt{1+\gamma_B^2}$. We shall discuss separately two limiting cases corresponding to $\gamma_1 > \Delta_Z B_0$ and $\gamma_1 < \Delta_Z B_0$. The first corresponds to a *weak mean field* with strong fluctuations and the second one to a *strong mean field* with weak fluctuations. For the numerical calculations we have chosen $\gamma_B = 1$, i.e. magnetic broadening equal to Doppler broadening, and $\Delta_Z B_0 = 0.1$ and $\Delta_Z B_0 = 3$, to represent the weak and strong mean field limits. The mean absorption and dispersion coefficients are calculated by numerical averaging over the PDF. In the limiting cases of weak and strong mean field, it is possible to obtain fairly simple analytical expressions for mean opacity and anomalous dispersion coefficients (see Paper I; also Dolginov & Pavlov 1972; Domke & Pavlov 1979). These analytic expressions are used to analyze the numerical results.

In this section we examine in detail the dependence of the mean residual Stokes profiles on the value of line strength β. The results are presented for β in the range 1 to 10^4. Very large values of β, around 10^4 can be found in magnetic white dwarfs (see for e.g. Martin & Wickramasinghe 1981, Nagendra & Peraiah 1985a,b, Wickramasinghe & Ferrario 2000). We assume that the mean magnetic field is in the longitudinal ($\theta_0 = 0°$) or in a transverse direction ($\theta_0 = 90°$, $\phi_0 = 0°$). Because the magnetic field fluctuations are isotropic, $\langle r_{\rm Q}\rangle = \langle r_{\rm U}\rangle = 0$ when $\theta_0 = 0°$ and $\langle r_{\rm V}\rangle = 0$ when

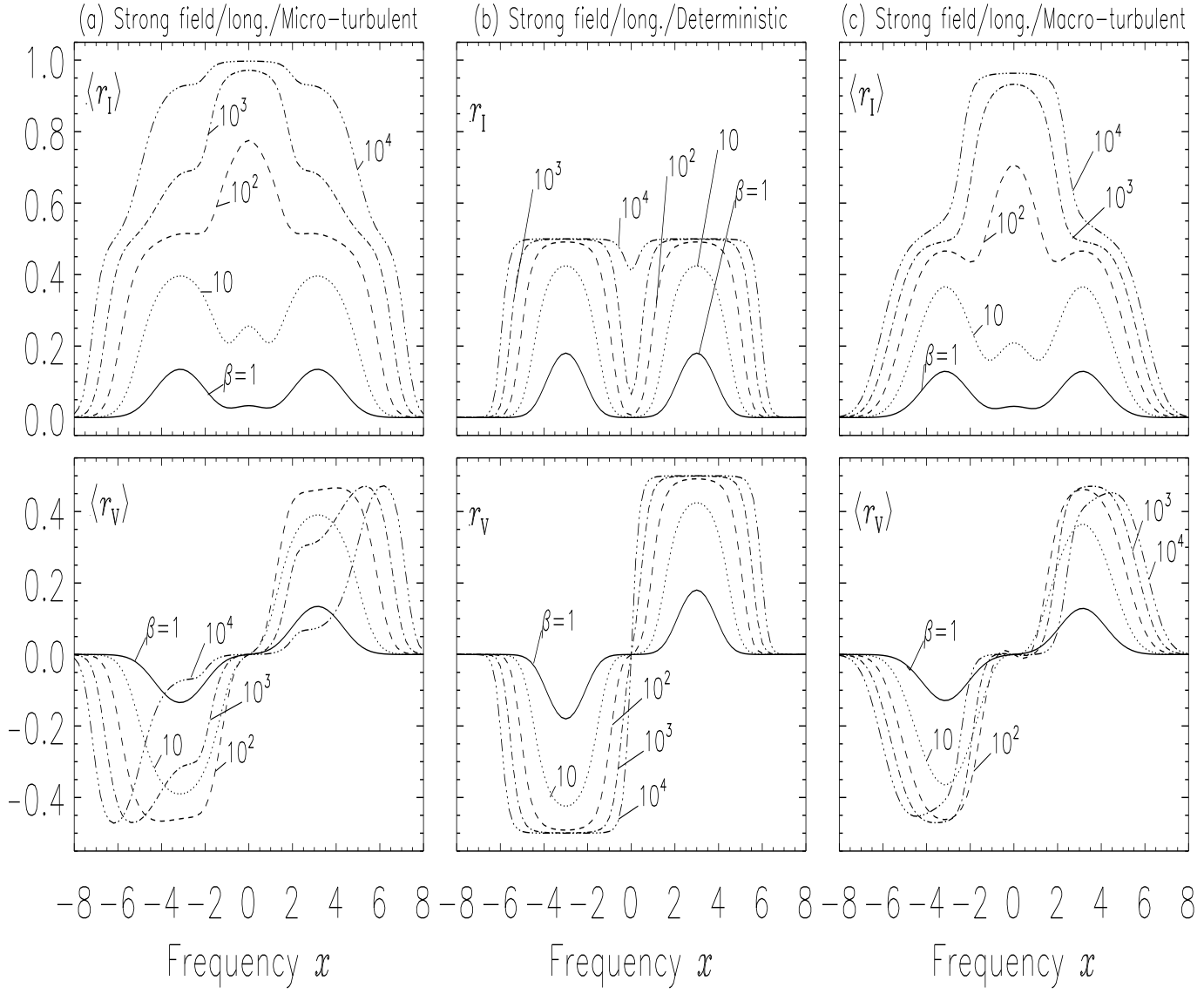

Fig. 2. Strong mean field limit. Longitudinal mean field case. Dependence of $\langle r_{\rm I}\rangle$, and $\langle r_{\rm V}\rangle$ on line strength β for $a = 0$, $\theta_0 = 0°$. Panel (a) : micro-turbulent limit with $\Delta_Z B_0 = 3$, $\gamma_B = 1$, hence $y_0 = 3$ and $f = 1/3$. Panel (b) : deterministic case with $\Delta_Z B = 3$. Panel (c) : macro-turbulent limit with the same model as in panel (a). See Sects. 2.2 and 3 for discussions.

$\theta_0 = 90°$, for symmetry reason. In addition $\langle r_{\rm U}\rangle = 0$ when $\phi_0 = 0°$. The notation $\langle\ \rangle$ stands for average over $P(\boldsymbol{B})$. All the calculations have been performed with a line damping parameter $a = 0$. Section 2.1 is devoted to the weak mean field limit, Sects. 2.2 and 2.3 to the strong mean field limit.

2.1. *Weak mean field (strong fluctuations) limit*

Figure 1a shows $\langle r_{\rm I}\rangle$, and $\langle r_{\rm V}\rangle$ for $\theta_0 = 0°$ calculated with Eqs. (A.14) and (A.15). When β is small ($\beta\langle\varphi_{\rm I}\rangle \ll 1$ for all x), one simply has $\langle r_{\rm I,V}\rangle \simeq \beta\langle\varphi_{\rm I,V}\rangle$. For large values of β, the shapes of $\langle r_{\rm I}\rangle$ and $\langle r_{\rm V}\rangle$ can be explained with the help of approximate expressions for $\langle\varphi_{\rm I,V}\rangle$. When $\gamma_1 > \Delta_Z B_0$, we have (see Paper I),

$$\langle\varphi_{\rm I}(x)\rangle \simeq \frac{1}{3}h^{(0)}(x) + \frac{2}{3\gamma_1^3}\left[h^{(0)}\left(\frac{x}{\gamma_1}\right) + 2\gamma_B^2 h^{(2)}\left(\frac{x}{\gamma_1}\right)\right], \quad (2)$$

$$\langle\varphi_{\rm V}(x)\rangle \simeq 2\Delta_Z B_0 \cos\theta_0 \frac{1}{\gamma_1^4}\left[h^{(1)}\left(\frac{x}{\gamma_1}\right) + \frac{2}{3}\gamma_B^2 h^{(3)}\left(\frac{x}{\gamma_1}\right)\right], \quad (3)$$

where $h^{(n)}(x) = x^n e^{-x^2}/\sqrt{\pi}$. When a is not zero, the $h^{(n)}$ functions become generalized Voigt functions $H^{(n)}$ (for details see Paper I; also Sampoorna et al. 2007). We remark that $\langle\varphi_{\rm I}\rangle$ is independent of θ_0 and $\langle\varphi_{\rm V}(x)\rangle$ of the order of $\Delta_Z B_0$. The mean values $\langle\varphi_{\rm Q}(x)\rangle$ and $\langle\varphi_{\rm U}(x)\rangle$ are of the order of $\Delta_Z B_0^2$ (see Paper I). The numerical results presented in Fig. 1a can be reproduced with an error less than 1%, when the approximations given in Eqs. (2) and (3) are combined with the expressions of $\langle r_{\rm I}\rangle$ and $\langle r_{\rm V}\rangle$ for $\Delta_Z B_0 < 1$ given in Eqs. (A.18) and (A.19).

The over all behavior of $\langle r_{\rm I,V}\rangle$ (namely, width of $\langle r_{\rm I}\rangle$, and peak position of $\langle r_{\rm V}\rangle$) can be explained by simple scaling arguments. For $\langle r_{\rm I}\rangle$, the width of the peak (Full width at Half Maximum FWHM) can be defined by the condi-

tion $\beta\langle\varphi_{\rm I}(x_{\rm c})\rangle \simeq 1$ with $x_{\rm c}$ the half-width. In Eq. (2) the terms with argument x/γ_1 are controlling the width of $\langle r_{\rm I}\rangle$, because they are decreasing more slowly with x than the $h^{(0)}(x)$ term. Hence $x_{\rm c} \sim \gamma_1\sqrt{\ln\beta}$. When $|x| < x_{\rm c}$, $\langle r_{\rm I}\rangle \to 1$ as $\beta \to \infty$ and when $|x| > x_{\rm c}$, $\langle r_{\rm I}\rangle$ behaves as $\beta\langle\varphi_{\rm I}\rangle$.

Equation (3) shows that the positions of the peaks of $\langle r_{\rm V}\rangle$ go like $\gamma_1\sqrt{\ln\beta}$ and their height goes as $\sqrt{\ln\beta}$. These predicted behaviors are very close to what is observed in the numerical results. For example the peak positions of $\langle r_{\rm V}\rangle$ scale as $1.5\sqrt{\ln\beta}$ whereas for our choice of parameters $\gamma_1 = 1.4$.

Comparison between the micro and mean field solution (see Fig. 1b), shows that magnetic turbulence produces a broadening of the peaks of $\langle r_{\rm I}\rangle$ and $\langle r_{\rm V}\rangle$ by a factor γ_1 and a decrease in amplitude of the $\langle r_{\rm V}\rangle$ peaks due to the factor $1/\gamma_1^4$ (see Eq. (3)).

When $\theta_0 = 90°$, the effects of a micro-turbulent magnetic field on $\langle r_{\rm Q}\rangle$ and $\langle r_{\rm U}\rangle$ are the same as for $\langle r_{\rm V}\rangle$, namely decrease in the amplitude of all three Zeeman components and broadening plus shifts in the positions of the σ-components away from line center.

2.2. *Strong mean field (weak fluctuations) limit. Longitudinal case*

Figure 2a shows $\langle r_{\rm I}\rangle$ and $\langle r_{\rm V}\rangle$ and Fig. 2b the corresponding curves for the mean field $\boldsymbol{B}_0$. It is clear that the profiles are quite different. We stress that the curves with $\beta = 1$ give a good approximation of the coefficients $\varphi_{\rm I}$ and $\varphi_{\rm V}$ and of their average values $\langle\varphi_{\rm I}\rangle$ and $\langle\varphi_{\rm V}\rangle$. Results presented in Fig. 2a can be understood using approximate (asymptotic) expression for $\langle\varphi_{\rm I,V}\rangle$. For $\gamma_1 < \Delta_Z B_0$, we have (see Paper I),

$$\langle\varphi_{\rm I}\rangle \simeq \bar\varphi_0 + \frac{1}{2}(\bar\varphi_{+1} + \bar\varphi_{-1}) + \frac{1}{2}(\bar c_{+1} + \bar c_{-1}), \quad (4)$$

$$\langle\varphi_{\rm V}\rangle \simeq \frac{1}{2}(\bar\varphi_{+1} - \bar\varphi_{-1}), \quad (5)$$

with

$$\bar\varphi_0 \simeq \frac{1}{2y_0^2}h^{(0)}(x);\ \bar\varphi_{\pm1}(x) \simeq \frac{1}{\gamma_1}\left(1 - \frac{1}{2y_0^2}\right)h^{(0)}(\bar x_{\pm1}), \quad (6)$$

$$\bar c_q(x) \simeq \frac{1}{4y_0^3}\frac{\gamma_1}{(y_0 + |xq|\gamma_B)}h^{(0)}(\bar x_q), \quad (7)$$

and $\bar x_q = (x - q\Delta_Z B_0)/\gamma_1$, $q = \pm1$. One notices in Eq. (4) the appearance of a term $\bar\varphi_0$ at line center which is zero for deterministic case (see Eq. (A.3) for $\theta = 0°$), and is created by the averaging of $\sin^2\theta$ over the random directions of the magnetic field. Equation (6) shows that the σ-components have a smaller amplitude and are broader by a scaling factor γ_1. The terms with $\bar c_q$ were not considered in the strong mean field limit expression for $\langle\varphi_{\rm I}\rangle$ of Paper I (see Eqs. (40) and (44) of Paper I). This term $\bar c_q$ comes from the factor $3/(4y_0^2 y)$ in Eq. (34) of Paper I. The expression given in Eq. (7) is an asymptotic expression for damping parameter $a = 0$. For $q = +1$, it is valid for x around y_0/γ_B and for $q = -1$, it is valid for x around $-y_0/\gamma_B$. In spite of being small compared to $\bar\varphi_q$, this term plays an important role around $x \simeq \pm\Delta_Z B_0$, when β is large. Using Eqs. (4) - (7) in Eqs. (A.14) and (A.15), we can reproduce the results presented in Fig. 2a to a good approximation.

When β becomes large, the quadratic terms in the denominator of the equations for $\langle r_{\rm I}\rangle$ and $\langle r_{\rm V}\rangle$ play an important role. For the analysis of the results, it is interesting to write the denominator as

$$d_{\rm l} \simeq 1 + 2\beta[\bar\varphi_0 + \frac{1}{2}(\bar\varphi_{+1} + \bar\varphi_{-1})] + \beta^2\{\bar\varphi_0^2 + [\bar\varphi_0 + \frac{1}{2}(\bar c_{+1} + \bar c_{-1})](\bar\varphi_{+1} + \bar\varphi_{-1}) + \bar\varphi_{+1}\bar\varphi_{-1}\}, \quad (8)$$

retaining only the leading terms.

In the upper panel of Fig. 2a we see that $\langle r_{\rm I}\rangle$ approaches 1 at line center and that this limiting value is almost reached for $\beta = 10^3$. At line center we have the exact relation

$$\langle r_{\rm I}(0)\rangle = \frac{\beta\langle\varphi_{\rm I}(0)\rangle}{1 + \beta\langle\varphi_{\rm I}(0)\rangle}, \quad (9)$$

hence $\langle r_{\rm I}(0)\rangle$ goes to one when $\beta\langle\varphi_{\rm I}(0)\rangle \gg 1$. Around the line center, $\langle\varphi_{\rm I}(x)\rangle \simeq \bar\varphi_0(x) \simeq e^{-x^2}/(\sqrt{\pi}2y_0^2)$ (see Eq. (6)). Hence, $\langle r_{\rm I}(0)\rangle \simeq 1$ when $\beta \gg \sqrt{\pi}2y_0^2$. For $y_0 = 3$, this condition yields $\beta \gg 30$, in agreement with the numerical results. It is the existence of a central component $\bar\varphi_0$ which is responsible for the very large difference between the micro-turbulent and the deterministic profiles.

The σ-components of $\langle r_{\rm I}(0)\rangle$ are well separated as long as $\beta \leq 10$, and their width is around $\gamma_1\sqrt{\ln\beta}$. For larger values of β, one notices a plateau with a value about 1/2 and then a further increase towards one. This can be understood by considering Eq. (8). At frequencies around $\Delta_Z B_0$, we have $\bar\varphi_{+1} \gg \bar\varphi_0 \gg \bar\varphi_{-1}$, hence

$$\langle r_{\rm I}(\Delta_Z B_0)\rangle \simeq 1 - \frac{\frac{\beta}{2}\bar\varphi_{+1}}{1 + \beta\bar\varphi_{+1} + \beta^2[\bar\varphi_0 + \bar c_{+1}/2]\bar\varphi_{+1}}. \quad (10)$$

The plateau around 1/2 is reached when $\beta\bar\varphi_{+1}/2 \gg 1$, i.e., when $\beta \gg 2\gamma_1\sqrt{\pi}$. Figure 2a shows that this plateau is reached for $10 < \beta < 10^2$, in agreement with the prediction. The saturation to one will occur when the term quadratic in β becomes larger than the linear term. This condition is satisfied when $\beta[\bar\varphi_0(\Delta_Z B_0) + \bar c_{+1}(\Delta_Z B_0)/2] \gg 1$. For our choice of parameters, this yields $\beta \gg 10^3$. Figure 2a shows that $\langle r_{\rm I}(\Delta_Z B_0)\rangle$ is close to one for $\beta = 10^4$. In the deterministic case $\bar\varphi_0 = 0$, hence the σ-components saturate to 1/2 as shown in Fig. 2b, upper panel.

The variations of $\langle r_{\rm V}\rangle$ with β are shown in lower panel of Fig. 2a. The σ-components tend to 1/2 when β increases, and their width goes as $\gamma_1\sqrt{\ln\beta}$. When the term $\beta^2[\bar\varphi_0 + \bar c_{+1}/2]\bar\varphi_{+1}$ becomes larger than $\beta\bar\varphi_{+1}$, a dip appears at frequencies $x \simeq \pm\Delta_Z B_0$. It becomes clearly visible when $\beta = 10^3$. For frequencies beyond $\pm\Delta_Z B_0$, the effect of $[\bar\varphi_0 + \bar c_{+1}/2]$ decreases, the term of order β^2 becomes small compared to the term of order β and $\langle r_{\rm V}\rangle$ goes to 1/2. Finally, $\langle r_{\rm V}\rangle$ goes to zero as $\beta\langle\varphi_{\rm V}\rangle$ when the frequency is

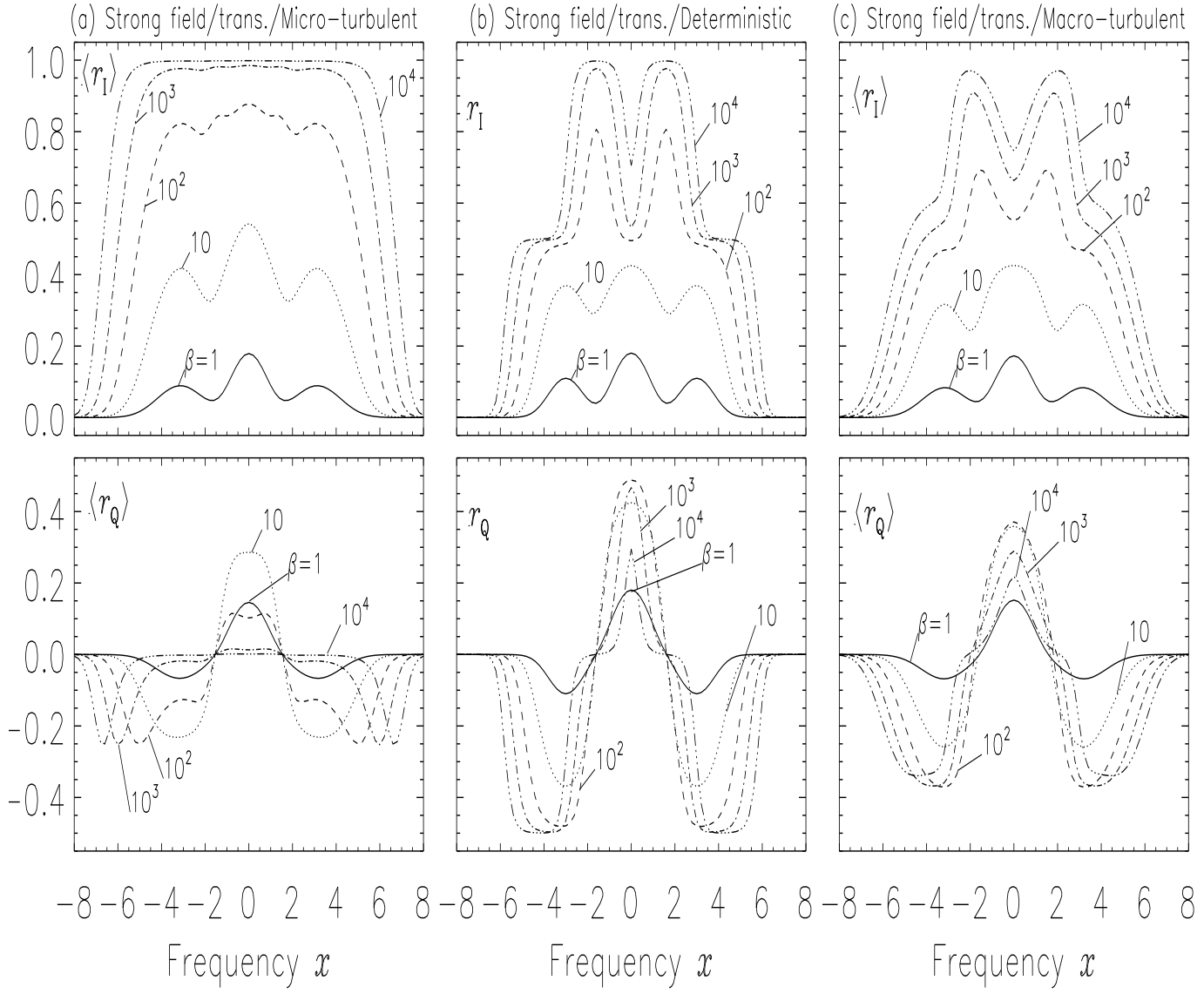

Fig. 3. Strong mean field limit. Transverse mean field case. Dependence of $\langle r_{\rm I}\rangle$, and $\langle r_{\rm Q}\rangle$ on line strength β for $a = 0$, $\theta_0 = 90°$, $\phi_0 = 0°$. Panel (a) : micro-turbulent limit with $\Delta_Z B_0 = 3$, $\gamma_B = 1$, hence $y_0 = 3$ and $f = 1/3$. Panel (b) : deterministic case with $\Delta_Z B = 3$. Panel (c) : macro-turbulent limit with the same model as in panel (a). See Sects. 2.3 and 3 for discussions.

large enough to give $d_{\rm l} \simeq 1$. The frequency at the peak, determined by the condition $\beta\langle\varphi_{\rm v}\rangle \simeq 1/2$, is about $|x| \simeq \Delta_Z B_0 + \gamma_1\sqrt{\ln\beta}$. Thus, for β sufficiently large, the peaks of $\langle r_{\rm V}\rangle$ lose their box like structure and the position of the maximum is essentially controlled by the parameter β and not by the Zeeman shift $\Delta_Z B_0$, unlike in the deterministic case (see Fig. 2b lower panel).

2.3. *Strong mean field (weak fluctuations) limit. Transverse case*

Figure 3a shows $\langle r_{\rm I}\rangle$ and $\langle r_{\rm Q}\rangle$ in the strong mean field (weak fluctuations) limit, for a mean field perpendicular to the LOS, i.e. $\theta_0 = 90°$. We also assume $\phi_0 = 0°$. Hence only $\langle\varphi_{\rm I}\rangle$ and $\langle\varphi_{\rm Q}\rangle$ are non zero. Figure 3b shows the corresponding curves calculated with the mean field. Again we observe a large difference between micro-turbulent and deterministic profiles.

To analyze the numerical results presented in Fig. 3a, we consider approximate expression for $\langle\varphi_{\rm I,Q}\rangle$. At leading order (see Paper I),

$$\langle\varphi_{\rm I}\rangle \simeq \frac{1}{2}(1-\frac{1}{2y_0^2})h^{(0)}(x) + \frac{1}{4\gamma_1}(1+\frac{1}{2y_0^2})[h^{(0)}(\bar{x}_{+1}) + h^{(0)}(\bar{x}_{-1})], \quad (11)$$

$$\langle\varphi_{\rm Q}\rangle \simeq \frac{1}{2}(1-\frac{3}{2y_0^2})h^{(0)}(x) - \frac{1}{4\gamma_1}(1-\frac{3}{2y_0^2})[h^{(0)}(\bar{x}_{+1}) + h^{(0)}(\bar{x}_{-1})]. \quad (12)$$

The terms $\bar{c}_q$ play no role in this case. The terms $3/2y_0^2$ and $1/2y_0^2$ are small compared to unity since $y_0 = 3$. However, when we consider the difference $\langle\varphi_{\rm I}\rangle^2 - \langle\varphi_{\rm Q}\rangle^2$ in the denominator of Eqs. (A.16) and (A.17) for $\langle r_{\rm I}\rangle$ and $\langle r_{\rm Q}\rangle$, these factors cannot be neglected. We thus have

$$d_{\rm t} \simeq 1 + 2\beta\langle\varphi_{\rm I}\rangle + \beta^2\Big\{\frac{1}{2y_0^2}[h^{(0)}(x)]^2 + \frac{1}{4\gamma_1^2 y_0^2}[h^{(0)}(\bar{x}_{+1}) + h^{(0)}(\bar{x}_{-1})]^2 + \frac{1}{2\gamma_1}h^{(0)}(x)[h^{(0)}(\bar{x}_{+1}) + h^{(0)}(\bar{x}_{-1})]\Big\}. \quad (13)$$

When β is sufficiently small, $d_{\rm t} \simeq 1$ and we recover the mean opacity coefficients $\beta\langle\varphi_{\rm I}\rangle$ and $\beta\langle\varphi_{\rm Q}\rangle$ which are fairly well represented by the curves corresponding to $\beta = 1$. We remark that the Eqs. (11) and (12), when used in Eqs. (A.16) and (A.17) for $\langle r_{\rm I}\rangle$ and $\langle r_{\rm Q}\rangle$ can reproduce the numerical result in Fig. 3a to a very good approximation.

With Eqs. (11) to (13) we can explain why $\langle r_{\rm I}\rangle$ approaches unity at all frequencies fairly rapidly when β increases. For x around the line center we can write

$$d_{\rm t} \simeq 1 + \beta h^{(0)}(x)\big[1 + \frac{\beta}{2y_0^2}h^{(0)}(x)\big], \quad (14)$$

and for x around the σ-components

$$d_{\rm t} \simeq 1 + \frac{\beta}{2\gamma_1}h^{(0)}(\bar{x}_{\pm1})\big[1 + \frac{\beta}{2y_0^2\gamma_1}h^{(0)}(\bar{x}_{\pm1})\big], \quad (15)$$

(the third term in the curly bracket in Eq. (13) can be neglected). The β^2-terms, which come from the small differences between the π and σ-components of $\langle\varphi_{\rm I}\rangle$ and $\langle\varphi_{\rm Q}\rangle$, (see Eqs. (11) and (12)) become relevant when $\beta/2y_0^2$ and $\beta/2y_0^2\gamma_1$ become of order or larger than unity. For our choice of parameters, this means that they play an important role when $\beta > 50$. This implies that the second term in Eq. (A.16) becomes small compared to unity because the numerator scales as β and the denominator as β^2. As a consequence $\langle r_{\rm I}\rangle$ goes to unity at line center and around the σ-components.

Roughly half-way between the π and σ-components , we have the point where $\langle\varphi_{\rm Q}\rangle = 0$. Around this frequency, denoted $x_{\rm m}$,

$$\langle r_{\rm I}(x_{\rm m})\rangle \simeq \frac{\beta\langle\varphi_{\rm I}(x_{\rm m})\rangle}{1 + \beta\langle\varphi_{\rm I}(x_{\rm m})\rangle}. \quad (16)$$

This expression rapidly approaches unity when β increases. Thus, when the mean field is in the transverse direction, $\langle r_{\rm I}\rangle$ approaches unity at line center, in the σ-components and half-way between these two regions. This explains the shape of the $\langle r_{\rm I}\rangle$ profiles shown in Fig. 3a, upper panel.

For $\langle r_{\rm Q}\rangle$, the micro-turbulent profile has qualitatively the same shape as the mean field profile (see lower panels in Fig. 3). There are however quantitative differences also due to the β^2-term in $d_{\rm t}$. At line center, when β is large, $\langle r_{\rm Q}\rangle$ is much smaller than the mean field solution. One observes also that the wing minima move away from line center to frequencies such that the β^2-term in $d_{\rm t}$ becomes negligible. Their positions vary roughly as $x \simeq \pm(\Delta_Z B_0 + \gamma_1\sqrt{\ln\beta})$. The amplitude of the minima are not very sensitive to the value of β and are approximately given by

$$\langle r_{\rm Q}\rangle \simeq \frac{\langle\varphi_{\rm Q}\rangle}{2\langle\varphi_{\rm I}\rangle} \simeq -\frac{1 - 3/2y_0^2}{1 + 1/2y_0^2} \simeq -0.4, \quad (17)$$

in fairly good agreement with the numerical results which yield $\langle r_{\rm Q}\rangle \simeq -0.35$.

3. Macro-turbulence with isotropic Gaussian fluctuations

We employ the isotropic Gaussian distribution already used to study the micro-turbulent limit (see Eq. (1)). We consider only the case of strong mean field with weak fluctuations ($\gamma_B = 1$, $\Delta_Z B_0 = 3$). We show in Figs. 2c and 3c the residual Stokes parameters for a longitudinal and a transverse mean field respectively. When the mean field is longitudinal, we have for symmetry reasons $\langle r_{\rm Q}\rangle = 0$ and $\langle r_{\rm U}\rangle = 0$. It is easy to check that Q and U average to zero when they are integrated over the azimuthal angle ϕ. When the mean field is in a transverse direction, i.e. when $\theta_0 = 90°$, averaging over an isotropic distribution yields $\langle r_{\rm V}\rangle = 0$. When in addition $\phi_0 = 0°$, one also has $\langle r_{\rm U}\rangle = 0$.

In the longitudinal case, as shown by Fig. 2c, $\langle r_{\rm I}\rangle$ behaves much as in the micro-turbulent case (see Fig. 2a, upper panel). A weak central component appears, which is created by the averaging over the angular distribution of the magnetic field. It is already visible when $\beta = 1$ and its value goes to unity when β increases. In the transverse case (see Fig. 3c), $\langle r_{\rm I}\rangle$ behaves essentially as in the deterministic case, except that the different components are somewhat broader and have a smaller value for the same value of β (compare upper panels of Fig. 3b, and 3c).

For $\langle r_{\rm V}\rangle$ (longitudinal case), the behavior is similar to the micro-turbulent limit, but for very large values of β ($\beta > 10^3$), the profiles are less distorted compared to the micro-turbulent case, and stay closer to the mean field value (see Fig. 2, lower panels). One can remark also that the position, height and shape of the peaks are largely independent of the value of β in a wide range of values ($1 < \beta < 10^3$).

For $\langle r_{\rm Q}\rangle$ (transverse case), we observe a shift of the positions of the minima away from the line center when β increases. It is stronger than in the deterministic case, but much weaker than in the micro-turbulent case (see Fig. 3, lower panels). Note also that the frequency at which $\langle r_{\rm Q}\rangle = 0$ depends slightly on β. This comes from the averaging process.

To summarize, for macro-turbulence the mean Stokes profiles of strong lines have a behavior which is similar to the micro-turbulent limit for the longitudinal case and similar to the mean field solution for the transverse case. For weak lines, $\beta \simeq 1$, or less, $\langle\boldsymbol{r}\rangle_{\rm micro} \simeq \langle\boldsymbol{r}\rangle_{\rm macro} \simeq \beta\langle\hat{\boldsymbol{\Phi}}\rangle\boldsymbol{U}$ as shown by Eqs. (A.23) and (A.24). Weak lines are not sensitive to the correlation length of the magnetic field.

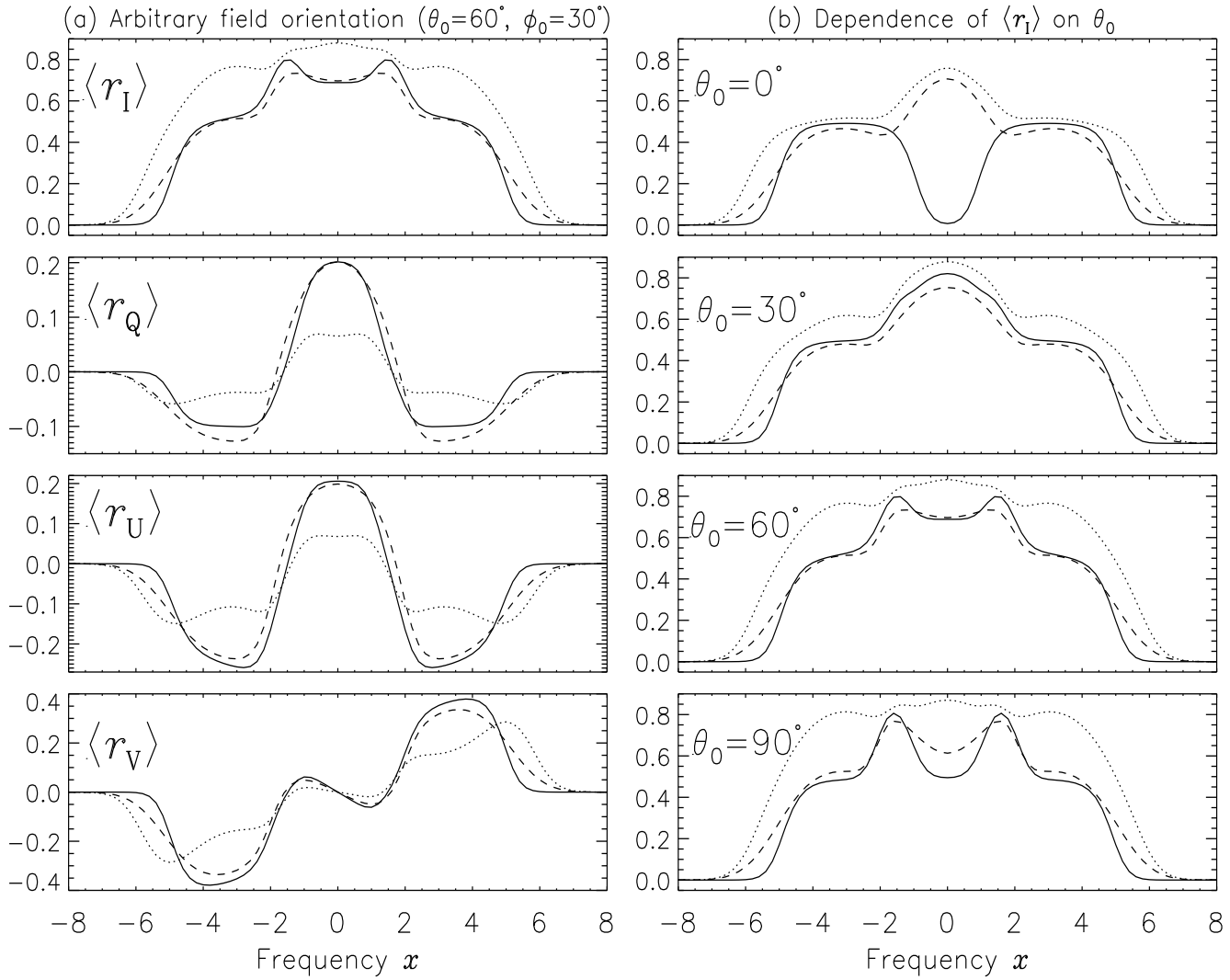

Fig. 4. UR solution for mean field (solid line), micro (dotted line), and macro (dashed line) limits. The line parameters are $a = 0$, and $\beta = 100$. Panel (a) : Mean magnetic field with parameters $\theta_0 = 60°$, $\phi_0 = 30°$, $\Delta_Z B_0 = 3$; weak magnetic field fluctuations ($\gamma_B = 1$). Panel (b) : dependence of $\langle r_{\rm I}\rangle$ on θ_0. The value of θ_0 is indicated in each sub-panel. See Sect. 4 for discussions.

4. Micro and macro-turbulent profiles for arbitrary orientation of the mean field

In this section we compare micro-turbulent, macro-turbulent and mean field solution Stokes profiles for a mean magnetic field with arbitrary orientation, and isotropic Gaussian fluctuations characterized by $y_0 = 3$, and $\gamma_B = 1$. This model corresponds to the strong mean field limit with weak fluctuations ($f = 1/3$). We know that for weak lines ($\beta \leq 1$), there are no differences between the micro and macro-turbulent limit and differences start showing up for $\beta = 10$, and they become quite large when β is around 100 or more. Hence the comparison is carried out for a spectral line with $\beta = 100$ and damping parameter $a = 0$.

Figure 4 shows the micro, macro and mean field Stokes profiles. In Fig. 4a we present $\langle r_{\rm I,Q,U,V}\rangle$ for $\theta_0 = 60°$, $\phi_0 = 30°$. The dependence of $\langle r_{\rm I}\rangle$ on field inclination θ_0 is shown in Fig. 4b. The behavior of $\langle r_{\rm Q,U,V}\rangle$ for micro-turbulent limit at π and σ-components is quite similar to that observed for longitudinal and transverse case (see lower panels of Figs. 2a and 3a). For example appearance of a dip at $x = 3$ and shifting of the σ-component peak position to a larger x are due to the dominance of the β^2 terms in the denominator of $\langle r_{\rm Q,U,V}\rangle$ (see Eqs. (A.7) - (A.13)).

For all the Stokes components the micro-turbulent profiles are broader than the macro-turbulent and mean field ones, and the difference between the macro and micro-turbulent profiles are large, except for the case $\theta_0 = 0°$. This phenomenon is illustrated for $\langle r_{\rm I}\rangle$ in the upper panel of Fig. 4b. The large difference between the turbulent and mean field profiles for large values of β have already been discussed in Sects. 2 and 3.

For an arbitrary orientation of the mean magnetic field, the exact and approximate expressions for the mean absorption and dispersion coefficients under strong field limit given in Paper I (see Eqs. (38) - (40)) give the numerical result presented in Fig. 4 (dotted line) to a very good approximation for $\theta_0 \neq 0°$. In the case of θ_0 around 0°, one

should also consider the term $\bar{c}_{\pm 1}$.

Another parameter which may affect the difference between the micro and macro-turbulent limits is the value of the damping parameter a. An increase in a produces a broadening and a decrease in magnitude of all the Zeeman components of the elements of the matrix $\hat{\mathbf{\Phi}}$ and as a consequence leads to a broadening and decrease in magnitude of all the Zeeman components of $r_{\rm Q,U,V}$, for turbulent as well as non-turbulent fields. For $r_{\rm I}$, the broadening of the Zeeman components may lead to the formation of a single peak.

5. Anisotropic magnetic field distributions

In the preceding sections we have considered a random magnetic field with isotropic distribution. For simplicity we refer to this model as 3D turbulence. This type of angular distribution can be considered as a reasonable approximation to magneto-hydrodynamic turbulence. Randomness of a quite different nature can be expected in sunspot umbra where thin flux tubes corresponding to umbral dots will probably be more or less oriented in the same direction (Thomas & Weiss 2004). In this case, the magnetic field fluctuates mainly in magnitude. For pure Gaussian intensity fluctuations Eq. (1) reduces to

$$P_{\rm L}(\boldsymbol{B})\, d\boldsymbol{B} = \frac{1}{\pi^{1/2}}\, e^{-(y-y_0)^2}\, dy, \quad -\infty < y < +\infty, \qquad (18)$$

a model which we refer to for simplicity as 1D or longitudinal turbulence. For 1D turbulence, the fluctuations of the magnetic field intensity affect the $q = \pm 1$ Zeeman components φ_q, but not the central component φ_0. The same is true for the anomalous dispersion coefficients.

Intermediate between isotropic and longitudinal fluctuations, as far as angular distribution is concerned, are fluctuations transverse to the mean field. The corresponding distribution function (see Paper I; also Domke & Pavlov 1979) may be written as

$$P_{\rm T}(\boldsymbol{B})\, d\boldsymbol{B} = \frac{1}{\pi}\, e^{-(y^2-y_0^2)} y\, dy\, d\Psi, \quad y_0 < y < +\infty. \qquad (19)$$

This case, referred here as 2D turbulence, is typical of Alfvén waves. When the intensity of the mean field is zero, this distribution can describe a magnetic canopy since the random magnetic field remains in a plane perpendicular to the direction (θ_0, ϕ_0).

We show in Fig. 5 the mean Stokes parameters for 1D, 2D and 3D turbulence in the micro-turbulent limit for a line with $\beta = 100$ and the same magnetic field model as in the preceding section ($\phi_0 = 30°$, $\theta_0 = 60°$, $\Delta_Z B_0 = 3$, $\gamma_B = 1$). The mean absorption and dispersion coefficients can be written explicitly in terms of the usual Voigt and Faraday-Voigt functions for 1D turbulence. For 2D turbulence they also have explicit expressions but for $a = 0$ only (see Paper I and also Domke & Pavlov 1979). Other numerical aspects of the calculation are presented in Frisch et al. (2006a,b).

The upper panel of Fig. 5 shows that amplitude of $\langle r_{\rm I}\rangle$ is fairly sensitive to the anisotropy of the distribution function. At line center, micro-turbulence always produces an increase in amplitude due to the broadening of the σ-components and to the averaging over the magnetic field directions, the latter mechanism being effective in the 2D and 3D cases only. Line center enhancement is present, for any value of θ_0 (see e.g. dotted lines in Fig. 4b). The magnitude of the σ-components is larger for 2D and 3D turbulence when compared to the mean field and 1D case because of the important role played by the β^2 terms.

For the polarization components, turbulence always broadens the Zeeman components and reduces their magnitude. For 1D turbulence, the π-component in $\langle r_{\rm Q,U}\rangle$ is reduced, and the σ-component in $\langle r_{\rm Q,U,V}\rangle$ are broadened compared to the mean field profiles. For $\langle r_{\rm Q}\rangle$ and $\langle r_{\rm U}\rangle$, 2D and 3D turbulence reduce the π and σ-component rather efficiently. For $\langle r_{\rm V}\rangle$, one can observe the same effect as for the σ-components of $\langle r_{\rm Q,U}\rangle$. The mean profiles for 2D and 3D turbulence are very similar, except for the width of the σ-components which are smaller for 2D than for 3D or 1D turbulence because the fluctuations are perpendicular to the mean field.

We also investigated the case of macro-turbulence. Compared to micro-turbulence, the averaged profiles stay closer to the mean field solution (see e.g. dashed lines in Fig. 4b).

6. Summary and concluding remarks

In this paper we take the example of a normal Zeeman triplet to explore the effects of a random magnetic field with mean value $\boldsymbol{B}_0$ on polarized line formation. The Unno–Rachkovsky solution which provides an explicit expression for the Stokes parameters at the surface of a Milne–Eddington atmosphere is used to calculate the mean Stokes parameters for random magnetic fields with scales of variations that are much smaller, or much larger than the mean free path of photons. These micro and macro-turbulent limits provide bounds for more general random magnetic fields with finite scales of variation. Thanks to the Unno–Rachkovsky (UR) solution, we could explore a broad range of magnetic field and spectral line parameters. For the spectral line, we varied the line strength β measured by the ratio of the line to continuum opacity.

For the random magnetic field $\boldsymbol{B}$, we have assumed Gaussian fluctuations about $\boldsymbol{B}_0$ given by a distribution function $P(\boldsymbol{B})$. Isotropic fluctuations and anisotropic ones (parallel and perpendicular to the mean field) are considered. The distribution is characterized by two Zeeman shifts : $\Delta_Z B_0$ due to the mean field and γ_B due to the rms fluctuations. The ratio $f = \gamma_B/\Delta_Z B_0$ provides a measure of the strength of the turbulent fluctuations. Most of the results concern a strong field/weak fluctuations limit ($\Delta_Z B_0 = 3$, $f = 1/3$).

In the micro-turbulent limit (Sect. 2), using explicit approximate expressions for the mean coefficients, we could follow in detail the variations of the Stokes profiles shapes

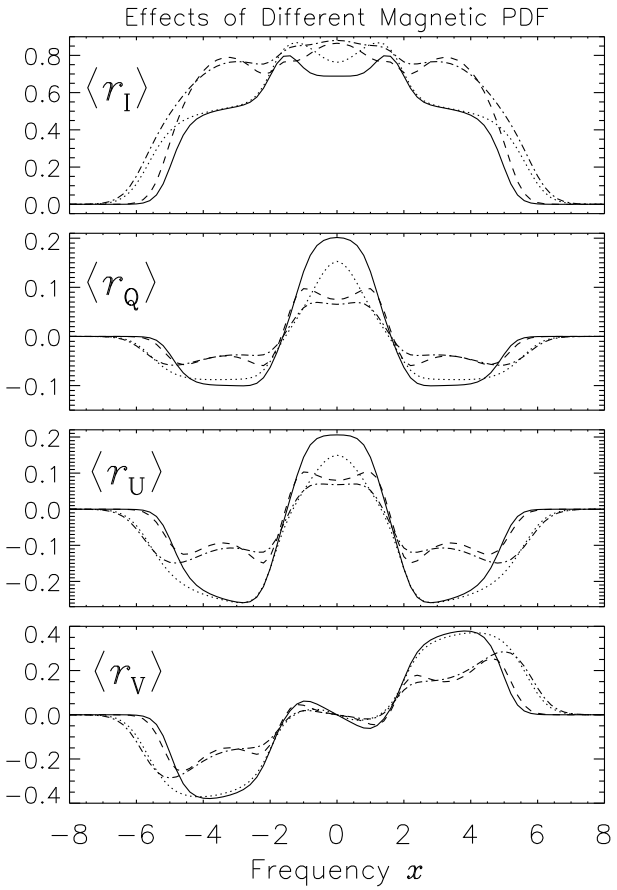

Fig. 5. Effects of different models of magnetic turbulence under micro turbulent limit. The solutions displayed are: deterministic mean field (solid line); 1D turbulence (dotted line); 2D turbulence (dashed line); 3D turbulence (dot-dashed line). The magnetic field parameters employed are same as in Fig. 4. See Sect. 5 for discussions.

as β increases and explain various saturation stages. These expressions along with the UR solution can predict Stokes profile that matches with the numerical result to a good approximation. For $\langle r_{\rm I} \rangle$ we have shown how fluctuations in the strength and direction of the magnetic field can produce an enhancement of the π-component which can lead, when β is large, to drastic changes in the profile shape as compared to the mean field solution.

In the macro-turbulent regime (see Sect. 3) the Unno–Rachkovsky solution is averaged over $P(\boldsymbol{B})$. Hence it is harder to perform a precise quantitative analysis of the mean profiles. Numerical calculations show that the macro-turbulent profiles have the same type of behavior as the micro-turbulent ones, but on the whole stay closer to mean field solutions.

Differences between the micro and macro-turbulent limits (see Sect. 4) are sensitive to the values of the damping parameter a and the line strength β. Non-existent for weak lines, say $\beta = 1$ or less, they become significant for $\langle r_{\rm I} \rangle$ when $\beta = 10$, but stay marginal for $\langle r_{\rm Q,U,V} \rangle$. They become really important only when β is around 100.

The sensitivity of the mean profiles to the angular distribution of the magnetic field is examined in Sect. 5 for a line with $\beta = 100$ and $a = 0$ and weak fluctuations ($f = 1/3$, $\Delta_Z B_0 = 3$). Micro-turbulent profiles are very sensitive to the choice of probability distribution function $P(\boldsymbol{B})$. The macro-turbulent profiles are however less sensitive than the micro-turbulent ones. It is a general feature of macro-turbulence in the case of weak fluctuations except for $\theta_0 = 0°$.

All the numerical results presented in this work have been obtained with a Gaussian distribution function. There is evidence for Voigt type distribution functions or stretched exponentials for the magnetic field intensity (see e.g. Stenflo & Holzreuter 2003; Stein & Nordlund 2006). The probability of magnetic fields deviating strongly from the mean field will be much larger in that case, than with a Gaussian distribution and hence stronger polarization and broader mean Stokes profiles are expected.

Acknowledgements

MS is financially supported by Council of Scientific and Industrial Research (CSIR), through a Senior Research Fellowship (SRF Grant No: 9/890(01)/2004-EMR-I), which is gratefully acknowledged. MS is also grateful to the Indo-French *Sandwich Thesis Program* for making possible a visit to the Observatoire de la Côte d'Azur. Further KNN and MS are grateful to the Laboratoire Cassiopée (CNRS), the PNST (CNRS) and the French Ministère de l'Éducation Nationale for financial support during visits at the Observatoire de la Côte d'Azur where part of this work was completed. HF was supported by the Indo-French Center for the Promotion of Advanced Research (IFCPAR 2404-2) and by the Indian Institute of Astrophysics during visits to Bangalore. The authors are grateful to anonymous referees for constructive comments.

References

Arena, P., Landi Degl'Innocenti, E., 1982. A&AS 48, 81.
Beckers, J.M., 1969. Solar Physics 9, 372
Bellot Rubio, L.R., 2006. In: Casini, R., Lites, B.W. (Eds.), Solar Polarization 4, ASP Conference Series, vol. 358, p. 107.
Carroll, T.A., Kopf, M., 2007. A&A 468, 323.
del Toro Iniesta, J.C., 2003. Introduction to Spectro polarimetry, Cambridge University Press, Cambridge.
Dolginov, A.Z., Pavlov, G.G., 1972. Soviet Ast. 16, 450 (transl. from Astron. Zhurnal, 49, 555, 1972)
Domke, H., Pavlov, G.G., 1979. AP&SS 66, 47
Frisch, H., Sampoorna, M., Nagendra, K.N., 2005. A&A 442, 11. (Paper I)
Frisch, H., Sampoorna, M., Nagendra, K.N., 2006a. A&A 453, 1095. (Paper II)
Frisch, H., Sampoorna, M., Nagendra, K.N., 2006b. In: Casini, R., Lites, B.W. (Eds.), Solar Polarization 4, ASP Conference Series, vol. 358, p. 126.

Frisch, H., Sampoorna, M., Nagendra, K.N., 2007. Mem. S. A. It. 78, 142.
Jefferies, J., Lites, B.W., Skumanich, A., 1989. ApJ 343, 920.
Landi Degl'Innocenti, E., 1976, A&AS 25, 379.
Landi Degl'Innocenti, E., Landolfi, M., 2004. Polarization in Spectral Lines, Kluwer Academic Publishers, Dordrecht.
Martin, B., Wickramasinghe, D.T., 1981. MNRAS 196, 23.
Mihalas, D., 1978. Stellar Atmospheres, 2nd ed., Freeman, San Francisco.
Nagendra, K.N., Peraiah, A., 1985a. MNRAS 214, 203.
Nagendra, K.N., Peraiah, A., 1985b. Ap&SS 117, 121.
Orozco Suárez, D., del Toro Iniesta, J.C., 2007. A&A 462, 1137.
Rachkovsky, D.N., 1962a. Izv. Krymsk. Astrofiz. Obs. 27, 148.
Rachkovsky, D.N., 1962b. Izv. Krymsk. Astrofiz. Obs. 28, 259.
Rees, D., 1987. In: Kalkofen, W. (Ed.), Numerical Radiative Transfer, Cambridge University Press, p. 213.
Sampoorna, M., Nagendra, K.N., Frisch, H., 2007. JQSRT 104, 71.
Sánchez Almeida, J., Landi Degl'Innocenti, E., Martinez Pillet, V., Lites, B.W., 1996. ApJ 466, 537.
Stein, R.F., Nordlund, Å., 2006. ApJ 642, 1246.
Stenflo, J.O., 1971. In: R. Howard (Ed.), Solar Magnetic Fields, IAU Colloq. 43, p. 101.
Stenflo, J.O., Lindegren, L., 1977. A&A 59, 367.
Stenflo, J.O., 1994. Solar Magnetic Fields, Kluwer Academic Publishers, Dordrecht.
Stenflo, J.O., Holzreuter, R., 2003. In: Pevtsov, A.A., Uitenbroek, H. (Eds.), Current Theoretical Models and Future High Resolution Solar observations: Preparing for ATST, ASP Conference Series, vol. 286, p. 169.
Thomas. J.H., Weiss, N.O., 2004. ARA&A 42, 517.
Unno, W., 1956. Publ. Astron. Soc. Japan 8, 108.
Wickramasinghe, D.T., Ferrario, L., 2000. PASP 112, 873.
Wittmann, A., 1974. Solar Physics 35, 11.

Appendix A. The Basic Equations

We consider a semi-infinite one-dimensional medium and to simplify notation concentrate on rays propagating in the direction normal to the surface. The radiative transfer equation for the Stokes vector $\boldsymbol{I} = (I, Q, U, V)^{\mathrm{T}}$ may then be written as

$$\frac{d\boldsymbol{I}}{d\tau_{\mathrm{c}}} = [\hat{\boldsymbol{E}} + \beta\hat{\boldsymbol{\Phi}}][\boldsymbol{I} - \boldsymbol{S}]. \tag{A.1}$$

Here τ_{c} is the continuum optical depth. The line strength parameter β and the 4×4 line propagation matrix $\hat{\boldsymbol{\Phi}}$ are constant. $\hat{\boldsymbol{E}}$ is the 4×4 identity matrix. The source term $\boldsymbol{S}$ has a linear variation given by $\boldsymbol{S}(\tau_{\mathrm{c}}) = (C_0 + C_1\tau_{\mathrm{c}})\boldsymbol{U}$ with $\boldsymbol{U} = (1, 0, 0, 0)^{\mathrm{T}}$, C_0 and C_1 being constants. In Fig. A.1 are defined the polar angles of the random and mean magnetic fields in a line of sight (LOS) reference frame.

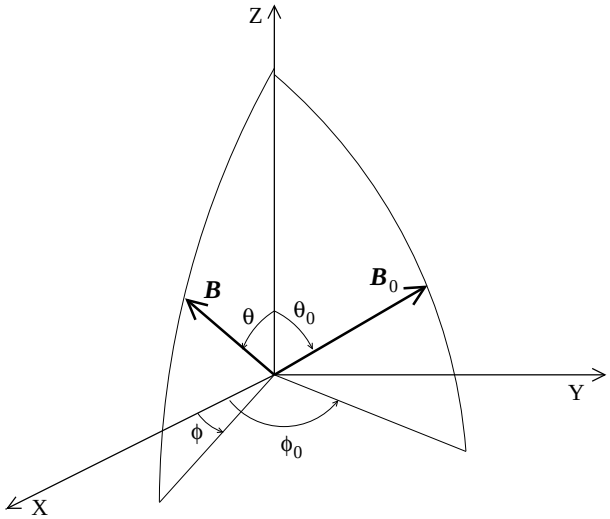

Fig. A.1. Line of sight (LOS) reference frame (X, Y, Z). The LOS is parallel to the Z-axis. The directions of random vector magnetic field $\boldsymbol{B}$ and mean magnetic field $\boldsymbol{B}_0$ are defined by the polar angles θ, ϕ and θ_0, ϕ_0 respectively.

The line propagation matrix can be written as (Landi Degl'Innocenti 1976; Rees 1987; Stenflo 1994)

$$\hat{\boldsymbol{\Phi}} = \begin{bmatrix} \varphi_{\mathrm{I}} & \varphi_{\mathrm{Q}} & \varphi_{\mathrm{U}} & \varphi_{\mathrm{V}} \\ \varphi_{\mathrm{Q}} & \varphi_{\mathrm{I}} & \chi_{\mathrm{V}} & -\chi_{\mathrm{U}} \\ \varphi_{\mathrm{U}} & -\chi_{\mathrm{V}} & \varphi_{\mathrm{I}} & \chi_{\mathrm{Q}} \\ \varphi_{\mathrm{V}} & \chi_{\mathrm{U}} & -\chi_{\mathrm{Q}} & \varphi_{\mathrm{I}} \end{bmatrix}. \tag{A.2}$$

For a normal Zeeman triplet, in the LOS reference frame, the absorption coefficients, $\varphi_{\mathrm{I,Q,U,V}}$ are given by

$$\begin{aligned} \varphi_{\mathrm{I}} &= \frac{1}{2}\varphi_0 \sin^2\theta + \frac{1}{4}(\varphi_{+1} + \varphi_{-1})(1 + \cos^2\theta), \\ \varphi_{\mathrm{Q}} &= \frac{1}{2}[\varphi_0 - \frac{1}{2}(\varphi_{+1} + \varphi_{-1})] \sin^2\theta \cos 2\phi, \\ \varphi_{\mathrm{U}} &= \frac{1}{2}[\varphi_0 - \frac{1}{2}(\varphi_{+1} + \varphi_{-1})] \sin^2\theta \sin 2\phi, \\ \varphi_{\mathrm{V}} &= \frac{1}{2}(\varphi_{+1} - \varphi_{-1}) \cos\theta, \end{aligned} \tag{A.3}$$

where φ_q ($q = 0, \pm 1$) are Voigt functions shifted by $q\Delta_B B$, with B the magnetic field strength. The anomalous dispersion coefficients $\chi_{\mathrm{Q,U,V}}$ are given by the same relations as $\varphi_{\mathrm{Q,U,V}}$ with Voigt functions replaced by Faraday-Voigt functions.

A.1. *Unno–Rachkovsky solution for deterministic fields*

According to the UR solution (see for e.g. Landi Degl'Innocenti 1976; Jefferies et al. 1989; Rees 1987) the surface value of the Stokes vector may be written as

$$\boldsymbol{I}(0) = [C_0 + C_1\hat{\boldsymbol{K}}^{-1}]\boldsymbol{U}, \tag{A.4}$$

where $\hat{\boldsymbol{K}} = \hat{\boldsymbol{E}} + \beta\hat{\boldsymbol{\Phi}}$. We introduce the vector

$$\boldsymbol{r}(0) = \frac{1}{C_1}[\boldsymbol{I}_{\rm c}(0) - \boldsymbol{I}(0)], \tag{A.5}$$

where

$$\boldsymbol{I}_{\rm c}(0) = (C_0 + C_1)\boldsymbol{U}, \tag{A.6}$$

is the continuum intensity at the surface. For simplicity we call $\boldsymbol{r}(0)$ the residual Stokes vector, although the usual residual Stokes vector, also called line depression Stokes vector (Stenflo 1994, p. 244), is defined by Eq. (A.5) with the intensity of the continuum $I_{\rm c}(0)$ in place of C_1.

The UR solution yields

$$r_{\rm I} = 1 - [\kappa_{\rm I}(\kappa_{\rm I}^2 + \rho_{\rm Q}^2 + \rho_{\rm U}^2 + \rho_{\rm V}^2)]/D, \tag{A.7}$$

$$r_{\rm Q} = [\kappa_{\rm I}^2\eta_{\rm Q} + \kappa_{\rm I}(\eta_{\rm V}\rho_{\rm U} - \eta_{\rm U}\rho_{\rm V}) + \rho_{\rm Q}W]/D, \tag{A.8}$$

$$r_{\rm U} = [\kappa_{\rm I}^2\eta_{\rm U} + \kappa_{\rm I}(\eta_{\rm Q}\rho_{\rm V} - \eta_{\rm V}\rho_{\rm Q}) + \rho_{\rm U}W]/D, \tag{A.9}$$

$$r_{\rm V} = [\kappa_{\rm I}^2\eta_{\rm V} + \rho_{\rm V}W]/D, \tag{A.10}$$

where

$$\kappa_{\rm I} = 1 + \beta\varphi_{\rm I};\ \eta_{\rm Q,U,V} = \beta\varphi_{\rm Q,U,V};\ \rho_{\rm Q,U,V} = \beta\chi_{\rm Q,U,V}, \tag{A.11}$$

$$W = \eta_{\rm Q}\rho_{\rm Q} + \eta_{\rm U}\rho_{\rm U} + \eta_{\rm V}\rho_{\rm V}, \tag{A.12}$$

$$D = \kappa_{\rm I}^2[\kappa_{\rm I}^2 - \eta_{\rm Q}^2 - \eta_{\rm U}^2 - \eta_{\rm V}^2 + \rho_{\rm Q}^2 + \rho_{\rm U}^2 + \rho_{\rm V}^2] - W^2. \tag{A.13}$$

We stress that W, D, $(\varphi_{\rm Q}^2 + \varphi_{\rm U}^2)$ and $(\chi_{\rm Q}^2 + \chi_{\rm U}^2)$ are independent of the azimuthal angle ϕ. Hence $r_{\rm I}$ and $r_{\rm V}$ are independent of ϕ whereas $r_{\rm Q}$ and $r_{\rm U}$ are ϕ-dependent. For $r_{\rm Q}$, the first and third term in the square bracket of Eq. (A.8) vary like $\cos 2\phi$ and the second term like $\sin 2\phi$. For $r_{\rm U}$, it is the first and third term which vary like $\sin 2\phi$ and the second term like $\cos 2\phi$.

UR solution takes a simpler form for longitudinal and transverse fields. When the magnetic field is aligned with the line of sight (longitudinal), the UR solution reduces to $r_{\rm Q} = r_{\rm U} = 0$ and

$$r_{\rm I} = 1 - \frac{1 + \beta\varphi_{\rm I}}{(1 + \beta\varphi_{\rm I})^2 - \beta^2\varphi_{\rm V}^2}, \tag{A.14}$$

$$r_{\rm V} = \frac{\beta\varphi_{\rm V}}{(1 + \beta\varphi_{\rm I})^2 - \beta^2\varphi_{\rm V}^2}, \tag{A.15}$$

with $\varphi_{\rm I} = (\varphi_{+1} + \varphi_{-1})/2$, $\varphi_{\rm V} = (\varphi_{+1} - \varphi_{-1})/2$.

When the magnetic field is in a transverse direction, the UR solution yields $r_{\rm V} = 0$, and

$$r_{\rm I} = 1 - \frac{1 + \beta\varphi_{\rm I}}{(1 + \beta\varphi_{\rm I})^2 - \beta^2(\varphi_{\rm Q}^2 + \varphi_{\rm U}^2)}, \tag{A.16}$$

$$r_{\rm Q,U} = \frac{\beta\varphi_{\rm Q,U}}{(1 + \beta\varphi_{\rm I})^2 - \beta^2(\varphi_{\rm Q}^2 + \varphi_{\rm U}^2)}, \tag{A.17}$$

where $\varphi_{\rm I} = [\varphi_0 + (\varphi_{+1} + \varphi_{-1})/2]/2$, and $\varphi_{\rm Q}^2 + \varphi_{\rm U}^2 = [\varphi_0 - (\varphi_{+1} + \varphi_{-1})/2]^2/4$. The zero-crossing points of $r_{\rm U}$ and $r_{\rm Q}$ correspond to $\varphi_{\rm Q} = \varphi_{\rm U} = 0$. They have frequencies $x = \pm x_{\rm m}$ with $x_{\rm m}$ defined by $\varphi_0(x_{\rm m}) = [\varphi_{+1}(x_{\rm m}) + \varphi_{-1}(x_{\rm m})]/2$. The value of $x_{\rm m}$ is independent of β.

When $\Delta_Z B \ll 1$, one can take $\varphi_{\rm I} \simeq \varphi_0 \simeq \varphi_{-1} \simeq \varphi_{+1}$. Equations (A.14) and (A.16) for $r_{\rm I}$, and Eqs. (A.15) and (A.17) for $r_{\rm V}$ and $r_{\rm Q}$ become

$$r_{\rm I} \simeq \frac{\beta\varphi_{\rm I}}{1 + \beta\varphi_{\rm I}}, \tag{A.18}$$

$$r_{\rm V} \simeq \frac{\beta\varphi_{\rm V}}{(1 + \beta\varphi_{\rm I})^2};\quad r_{\rm Q,U} \simeq \frac{\beta\varphi_{\rm Q,U}}{(1 + \beta\varphi_{\rm I})^2}, \tag{A.19}$$

with

$$\varphi_{\rm V} \simeq -\Delta_Z B\frac{d\varphi_{\rm I}}{dx};\quad \varphi_{\rm Q} \simeq -\frac{1}{4}\Delta_Z B^2\frac{d^2\varphi_{\rm I}}{dx^2}. \tag{A.20}$$

A.2. *Unno–Rachkovsky solution for turbulent fields*

In the macro-turbulent and micro-turbulent regimes, the UR solution becomes

$$\langle\boldsymbol{I}(0)\rangle_{\rm macro} = [C_0 + C_1\langle\hat{\boldsymbol{K}}^{-1}\rangle]\boldsymbol{U}, \tag{A.21}$$

$$\langle\boldsymbol{I}(0)\rangle_{\rm micro} = [C_0 + C_1\langle\hat{\boldsymbol{K}}\rangle^{-1}]\boldsymbol{U}, \tag{A.22}$$

where the angle brackets denote the average over the distribution function of the vector magnetic field $P(\boldsymbol{B})$. The mean residual Stokes vector for macro and micro-turbulent regimes are respectively,

$$\langle\boldsymbol{r}(0)\rangle_{\rm macro} = \langle\beta\hat{\boldsymbol{\Phi}}[\hat{\boldsymbol{E}} + \beta\hat{\boldsymbol{\Phi}}]^{-1}\rangle\boldsymbol{U}, \tag{A.23}$$

$$\langle\boldsymbol{r}(0)\rangle_{\rm micro} = \beta\langle\hat{\boldsymbol{\Phi}}\rangle[\langle\hat{\boldsymbol{E}} + \beta\hat{\boldsymbol{\Phi}}\rangle]^{-1}\boldsymbol{U}. \tag{A.24}$$

The methods to perform the averaging efficiently in the micro and macro-turbulent limits are presented in Frisch et al. (2006a) (see also Frisch et al. 2005, 2006b).